Applied Mathematics & Information Sciences
An International Journal

http://dx.doi.org/10.18576/amis/190409

Interlayer Synchronization in Multiplex Networks of Coupled Discrete Duffing Oscillators and Application to Cryptography

Ahamat Mahamat Hassane[1,3,4], *Kalsouabe Zoukalne*[1,3,4], *Yaya Dagal Dari*[5] *and Paul Woafo*[1,2,*]

[1]Laboratory on Modelling and Simulation in Engineering, Biomimetics and Prototypes, and TWAS Research Unit, Faculty of Science, University of Yaoundé I, Box 812, Yaoundé, Cameroon
[2]Laboratory of Products Development and Entrepreneurship, Institut Supérieur de l'Innovation et de Technologie, P.O. Box 8210 Yaoundé, Cameroon
[3]Techno-pedagogy Unit, Virtual University of Chad, Box 5711, N'Djamena, Chad
[4]Physics and Engineering Science Training, Sciences-Technology-Environment Doctoral School, University of N'Djamena, Box 1117, N'Djamena, Chad
[5]National Institute of Sciences and Techniques of Abeche (INSTA), Chad

Received: 2 Dec. 2024, Revised: 12 Feb. 2025, Accepted: 31 Mar. 2025
Published online: 1 Jul. 2025

Abstract: The synchronization of discrete simple and extended Duffing oscillators in three-layer network is investigated in this paper. Discrete simple and extended one-dimensional Duffing oscillators are characterized to determine the control parameters inducing chaotic behaviors. The effects of the fractional derivative on the bifurcation diagrams of these discrete oscillators are also analyzed. In addition, the coupling domain of interlayer forces leading to synchronization in the three-layer network is determined numerically. Finally, chaos synchronization in three-layer network of discrete simple and extended Duffing oscillators is used for chaotic message cryptography.

Keywords: Discrete Duffing oscillators, fractional derivative, chaos, multiplex networks, synchronization, chaos cryptography.

1 Introduction

In the field of nonlinear physics, synchronization is a crucial phenomenon that is the subject of numerous studies. It can be found in various fields such as engineering [1], fundamental physics [2] and biology [3]. Given the applications it offers, the synchronization of networks of layered chaotic oscillators is of great interest [4]. When several oscillators interact, various dynamic states can occur. These dynamic states depend on the number of oscillators and the type and strength of the coupling [5]. In complex networks, synchronization can be partial [6], complete [7] or by relay [8,9]. In order to account for these different levels of interaction in complex systems, the concept of multi-layer networks was developed during the previous decade[10,11,12]. A multilayer network is made up of several interacting sub-networks, a sub-network being a layer of the larger network. For the past decade, synchronization phenomena have been studied in multilayer networks [13,14,15,16,17]. A mathematical formulation for the study of multilayer networks was presented in [18]. Rybalova et al [19] found complete relaying and synchronization in heterogeneous multiplex networks. Inter-layer synchronization in non-identical multilayer networks was presented in [20]. This study showed that the divergence of interlayer synchronization depends on the strength of the coupling.

The application of chaos to telecommunication systems has been possible ever since the synchronization of chaotic systems came into being. Chaotic synchronization, with its inherent non-linearity and dependence on initial conditions, is of great interest for secure communications [21,22,23,24], where data security and integrity cannot be compromised at any cost. Several schemes for encoding and decoding a message

* Corresponding author e-mail: pwoafo1@yahoo.fr

using chaotic signals have been proposed in the literature [25,26,27,28], including encryption/decryption based on multilayer network synchronization [29,30,31,32], which is currently attracting particular attention from researchers.

In the present work, motivated by the opportunity offered by the synchronization of the referenced works, we analyze the dynamic behavior and synchronization in a three-layer network of coupled simple Duffing, then coupled extended Duffing discrete oscillators considering also the effects of the fractional derivative. The effects of coupling strength on the synchronization of these three layers are analyzed. We then apply this synchronization of coupled simple Duffing oscillators to chaotic cryptography for information masking.

The sections of this paper are as follows. Section 2 presents the characterization of the simple and extended Duffing discrete oscillators in their control parameters planes. In section 3, the effects of the fractional derivative is considered. In Section 4, the synchronization of simple and extended Duffing discrete oscillators in a 3-layer network is analyzed. In Section 5, the chaotic single and extended Duffing states of the network are used in chaotic cryptography for information hiding. Section 6 is the conclusion.

2 Characterization of the simple Duffing discrete oscillator and the extended Duffing discrete oscillator

2.1 Characterization of the simple Duffing discrete oscillator

The discrete Duffing oscillator is described by equation (1)[33].

$$\begin{cases} x(n+1) = y(n) \\ y(n+1) = -\beta x(n) + \alpha y(n) - y(n)^3 \end{cases} \tag{1}$$

where y and x are real observables, n is the discrete time. β and α are the system coefficients. We have characterized the dynamical behaviour of the Duffing oscillator in the (α, β) parameters space. This appears in Fig. 1 where the blue hatched area indicates the pairs of parameters (α, β) leading to chaos while the white area corresponds to the domain where the discrete Duffing oscillator generates periodic sequences and non-oscillatory constant states. One finds an almost triangular domain where chaos is present.

In Figure 2, we plot a representative of the bifurcation diagram versus the parameter α. This is accompanied by the corresponding variation of the Lyapunov exponent. One finds that a periodic state is present for small values of the parameter α comprises between 2.35 and 2.4. A series of period doubling bifurcation takes place and ends at approximately α=2.663 and chaos takes place. This transition to chaos is ascertained by the variation of the Lyapunov exponent which becomes positive when chaos is present.

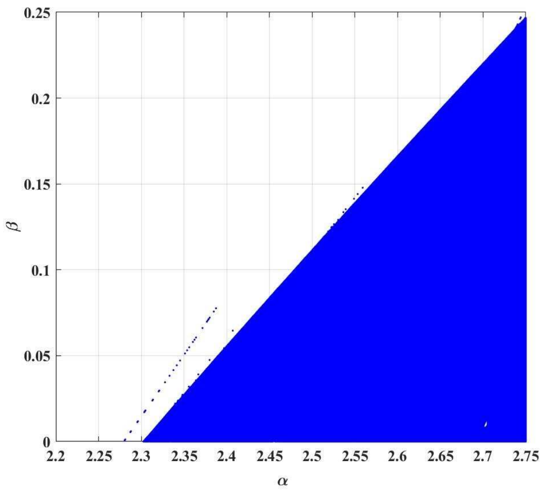

Fig. 1: Bifurcation diagram in the (α, β) plane for the discrete Duffing oscillator. The blue region corresponds to domain of control parameters leading to chaos.

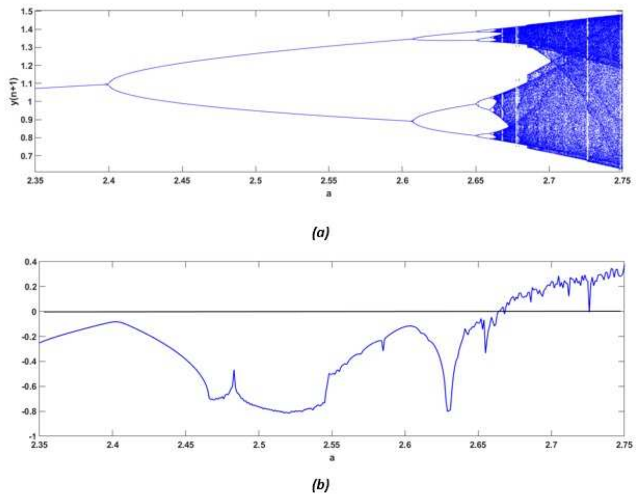

Fig. 2: Bifurcation diagram versus α (a) and Lyapunov exponent (b) of the Duffing map for β =0.2.

To highlight more the dynamical states appearing in Figures 1 and 2, we have also plotted some time traces. The periodic state is present in Fig. 3(a) for α=2.39 and β=0.1. For α=2.75 and β=0.2, we observe a totally chaotic state as shown in Fig. 3 (b). Fig. 4 presents the phase portrait for α=2.75 and β=0.2 for which chaos is present.

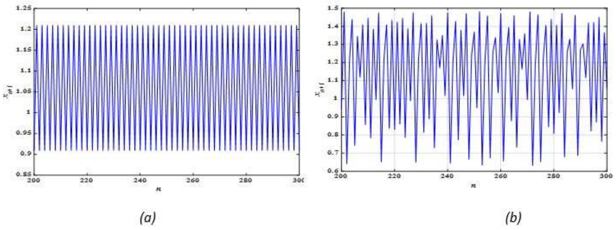

Fig. 3: Time-histories of the discrete Duffing oscillator when α=2.39 and β=0.1 (a); α=2.75 and β=0.2 (b).

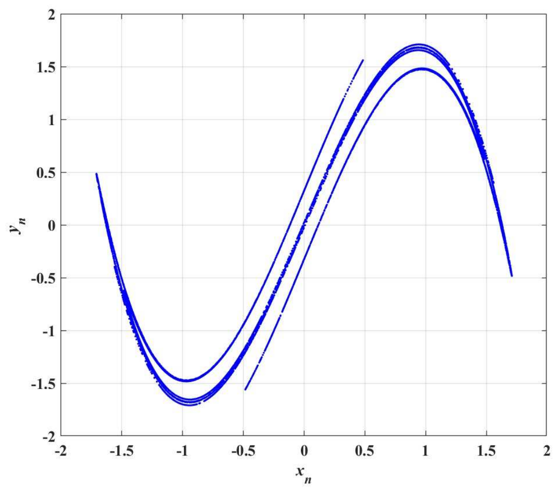

Fig. 4: Phase portrait when α=2.75 and β=0.2.

2.2 Characterization of the extended Duffing discrete oscillator

We have introduced additional terms into equation 1 to include more complex physical effects such as higher-order nonlinearities (y^5) and a new control parameter (d). The extended Duffing equation becomes:

$$\begin{cases} x(n+1) = y(n) \\ y(n+1) = -\beta x(n) + \alpha y(n) - y(n)^3 + dy(n)^5 \end{cases} \tag{2}$$

We have characterized the dynamic behavior of the extended Duffing oscillator (equation 2) in (d,β) parameter space. Figure 5 presents the results where the blue hatched area indicates the (d,β) parameter pairs that lead to chaos, while the white area presents the region where the discrete Duffing oscillator produces periodic sequences and constant non-periodic states. We observe an almost triangular area where chaos manifests itself and also when d grows, the chaotic domain following β decreases until disappearing for d around 0.09.

Figure 6 shows a bifurcation diagram as a function of parameter d, together with the associated variation in the

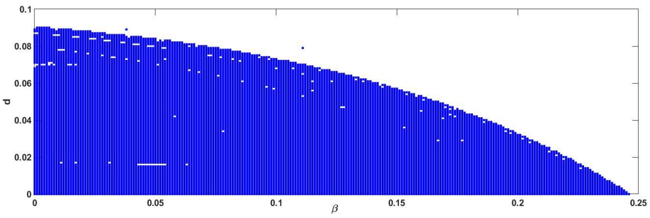

Fig. 5: Bifurcation diagram in the (d,β) plane with a=2.75.

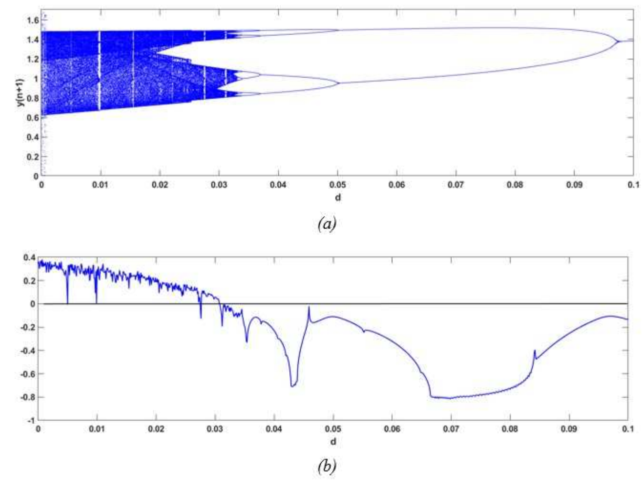

Fig. 6: Bifurcation diagram versus d (a) and Lyapunov exponent (b) of the Duffing map for α=2.75 and β=0.2.

Lyapunov exponent. It can be seen that the chaotic zone is represented on the interval from 0 to 0. 0.033. Then a series of period division takes place leading to periodic oscillation for d values between 0.0329 and 0.1. This transition to periodic or oscillatory states is evidenced by the change in sign of the Lyapunov exponent, which turns out to be negative.

3 The fractional order discrete Duffing extended oscillators

In order to extend the characterization of the discrete Duffing oscillators, our analysis has considered their fractional order forms. The Grünwald-Letnikov formulation [34] has been used. In particular, this section focuses on how the dynamical behavior and the appearance of chaotic attractors in the simple and extended Duffing maps are influenced by the introduction of fractional orders.

3.1 Development in fractional order

The Grünwald-Letnikov difference of fractional order is given by the relation 3 [34].

$$\Delta^{\gamma}x(n)=\sum_{j=0}^{n}(-1)^{j}\binom{\gamma}{j}x(n-j) \tag{3}$$

Where $\gamma \in R$ is the fractional order and the binomial coefficient is defined as follows:

$$\binom{\gamma}{j}=\begin{cases}0 & \text{if } j=0\\ \frac{\gamma(\gamma-1)(\gamma-2)\ldots(\gamma-j+1)}{j!} & \text{si } j>0\end{cases} \tag{4}$$

By extending the previous fractional order difference, we obtain the following relationship:

$$\Delta^{\gamma}x(n+1)=x(n+1)-x\gamma(n)+\sum_{j=2}^{n+1}(-1)^{j}\binom{\gamma}{j}x(n-j+1) \tag{5}$$

In order to simplify equation 5, we put m = j − 1, and it becomes

$$\Delta^{\gamma}x(n+1)=x(n+1)-\gamma x(n)+\sum_{m=1}^{n}(-1)^{m+1}\binom{\gamma}{m+1}x(n-m) \tag{6}$$

Let's put $C_m=(-1)^{m+1}\binom{\gamma}{m+1}$, then the fractional order difference is given in equation 7 [35]:

$$\Delta^{\gamma}x(n+1)=x(n+1)-\gamma x(n)+\sum_{m=1}^{n}C_{m}x(n-m) \tag{7}$$

By applying fractional order difference to the system of discrete integers such as : x(k+1) = f(x(k)) where f is a non-linear function, we obtain equation [34].

$$\Delta^{\gamma}x(n+1)=x(n+1)-x(n) \tag{8}$$

Equation 5 and equation 7 give the general formula 9:

$$x(n+1)=f(x(n))+(\gamma-1)x(n)-\sum_{m=1}^{n}C_{m}x(n-m) \tag{9}$$

As established in references [36,37], as n increases, *Cm* decreases. This makes computations less efficient and the number of states becomes a difficult number to store, since the actual memory of machines is limited. To solve this problem, we use a finite approximation to study a discrete-time system of fractional order. Considering L as the finite approximation, equation 9 becomes :

$$x(n+1)=f(x(n))+(\gamma-1)x(n)-\sum_{m=1}^{L}C_{m}x(n-m) \tag{10}$$

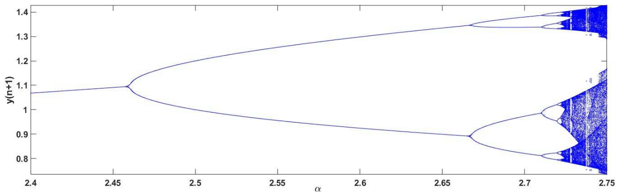

Fig. 7: Simple Duffing bifurcation diagram with fractional order with β=0.2 and γ=0.94.

Applying this formula to the simple and extended Duffing equations, we obtain equations 11 and 12 respectively:

$$\begin{cases}x_{n+1}=y(n)\\ y_{n+1}=-\beta x(n)+\alpha y(n)-y(n)^{3}+(\gamma-1)y(n)-\\ \sum_{m=1}^{L}C_{m}y(n-m)\end{cases} \tag{11}$$

$$\begin{cases}x_{n+1}=y(n)\\ y_{n+1}=-\beta x(n)+\alpha y(n)-y(n)^{3}+dy(n)^{5}+(\gamma-1)y(n)\\ -\sum_{m=1}^{L}C_{m}y(n-m)\end{cases} \tag{12}$$

3.2 Analysis of the influence of the fractional derivative on simple Duffing bifurcation diagrams

We illustrate the bifurcation diagrams of the simple Duffing system at fractional order for fractional coefficients of 0.94 and 0.98 respectively in Fig.s 7 and 8. Comparing this result with the simple Duffing bifurcation diagram without the fractional derivative in Fig. 2, we note that when the fractional order is small the area of the chaos zone is reduced. When the fractional order coefficient is slightly large, the size of the chaotic regions almost approaches that of simple Duffing without fractional order. However, the locations of the periodic windows are adjusted. More explicitly, Fig. 8, which illustrates the bifurcation of simple Duffing with a fractional derivative (γ=0.98), shows that the interval 2.4 to 2.683 exhibits periodic states. Beyond this interval, chaos sets in, with a first periodic window when α = 2.688, followed by further periodic windows (α=2.698, α=2.745).

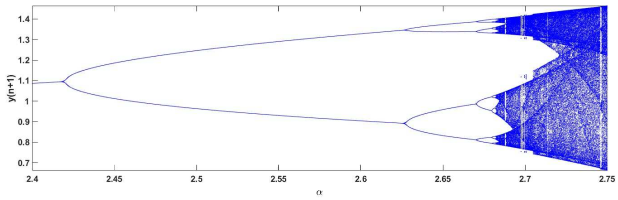

Fig. 8: Simple Duffing bifurcation diagram with fractional order with β=0.2 and γ=0.98.

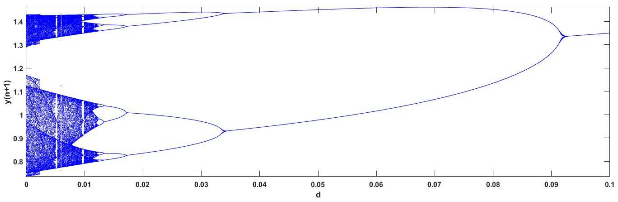

Fig. 9: Expanded Duffing bifurcation diagram with fractional order with α=2.75,β=0.2 and γ=0.94.

3.3 *Analysis of the influence of the fractional derivative on extended Duffing bifurcation diagrams*

Fig.s 9 and 10 shows the bifurcation diagram of the fractional-order extended Duffing system for fractional order coefficients of 0.94 and 0.98 respectively. If we compare these Fig.s with the bifurcation diagram of extended Duffing without fractional order (Fig. 6), we see that a small fractional order reduces the surface area in the chaotic zone. When the fractional order coefficient is slightly large, the size of the chaotic zones is almost the same as that of the extended Duffing without fractional order. However, the positions of the periodic windows change. More clearly, in Fig. 10, which shows the bifurcation of extended Duffing with fractional derivative (γ=0.98), the chaotic interval is repeated from 0 to 0.026. Over this interval, the first periodic window is observed when d= 0.0017, followed by other periodic windows (d=0.0077, d=0.00207, d=0.024). An inverse period doubling is observed beyond d= 0.026. This doubling disappears as the value of d increases, down to a single period when d= 0.095.

Comparing the above results with other works in the literature, it is noted that the behaviors observed on the fractional-order simple and extended Duffing maps are almost identical to those observed on the fractional-order Ueda map [38] and the logistic map [35]. Indeed in these mentioned references, it is known that the fractional order coefficient modifies the domains for periodic and chaotic dynamics. This corresponds to an additional control parameter which can be useful for the control of chaos and for the optimization for application to chaotic cryptography [35].

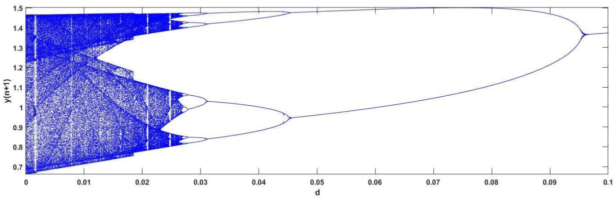

Fig. 10: Expanded Duffing bifurcation diagram with fractional order with α=2.75,β=0.2 and γ=0.98

4 Study of the synchronization of coupled simple and extended Duffing oscillators in a three-layer network

4.1 *Study of the synchronization of coupled single-duffing oscillators in a three-layer network*

In this part of the work, we study a network with three distant layers of time-discrete Duffing oscillators. In each layer, when there is no coupling, all the oscillators are in a temporal chaotic state. We present scenarios for synchronizing these three distant layers coupled by a coupling force σ_{ml}, and then discuss the transition between coherent and incoherent domains in this 3-layer network. The three coupled layers are described by equations 13.

$$\begin{cases} x_i^m(n+1) = f_x^m(x_i,y_i) = y_i^m(n) \\ y_i^m(n+1) = f_y^m(x_i,y_i) + \frac{\sigma_m}{2P_m}\sum_{j=i-P_m}^{i+P_m}\left[f_y^m(x_j,y_j) - f_y^m(x_i,y_i)\right] \\ +\sum_{l=1}^{3}\sigma_{ml}\left[f_y^l(x_i,y_i) - f_y^m(x_i,y_i)\right] \end{cases} \tag{13}$$

The superscript $m = 1,2,3$ corresponds to the number or rank of the layer. $\boldsymbol{P_m}$ is the non-local intra-layer coupling related to the coupling radius $r_m = \frac{P_m}{N}$, σ_{m} is the intra-layer coupling force. σ_{ml} is the inter-layer coupling force. The total number of oscillator is N = 300. The value of $\boldsymbol{P_m}$ is 90 . To study the synchronization between two layers 1, m, the interlayer synchronization error Eml will be used. It is defined by equation 14.

$$E_{ml} = \lim_{T\to\infty}\frac{1}{NT}\sum_{t=0}^{T}\sum_{i=1}^{N}\left\|y_i^l(n) - y_i^m(n)\right\| \tag{14}$$

Where $||-||$ is the Euclidean norm and T is the number of time steps. For synchronization, we need to measure the synchronization error between the first and third layers E13 and between the first and second layers E12. Thus, global synchronization occurs when E13 = 0 and E12 = 0 [17].

To determine where the layers are synchronized, we need to measure the synchronization error between the first and second layers (E12) and the synchronization error between the first and third layers (E13). Fig.11

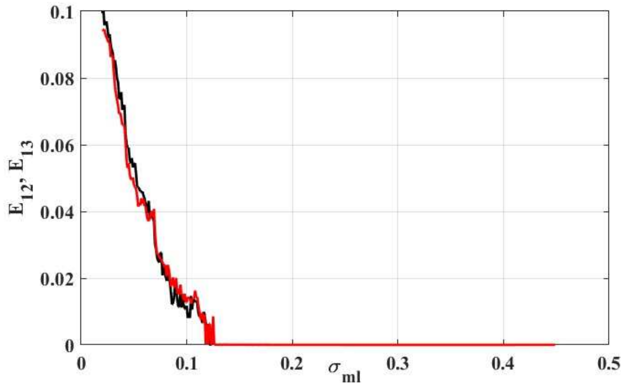

Fig. 11: Synchronization error between first and second layer (E12) and between first and third layer (E13) as a function of interlayer coupling strength σ_{ml}.

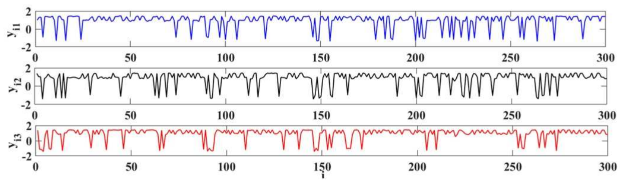

Fig. 12: 3-layer desynchronization. n=40500, σ_{ml}= 0,05, σ_{m}= 0,26, β=0.2 ,α=2.75, P_m=90 ,i=0 à N (with N=300) the initial conditions are chosen randomly between 0 and 1.

shows that when the synchronization errors E12 and E13 are zero, the 3 layers are synchronized with each other; if they are not zero, there will be no synchronization. To confirm these measurements, we take two values of σ_{ml} (one when Eml is zero and one for Eml different from zero) to plot the spatial traces *yi* as a function of *i* and the temporal traces *yi* as a function of *n*.

For a value of σ_{ml} = 0.05, the spatial traces (Fig. 12) show that these three layers are not synchronized. This can be seen in the dynamic behavior of each layer (yi1, yi2 and yi3). Each layer has different dynamics. The oscillators of each layer follow their own dynamics, indicating desynchronization despite the low coupling force applied. To confirm the scenarios in Fig. 12, time traces are plotted in Fig. 13. The focus is on oscillator no.150 of each layer. The oscillations shown in Fig. 13 (blue, black and red) exhibit chaos, reflecting independent dynamic states between the layers.

In Fig.14, the results show that for a value of σ_{ml}=0.25, the three layers are synchronized with each other. This can be seen in the dynamic behavior of each layer (yi1, yi2 and yi3). The oscillators of these three layers produce the same dynamic behavior showing complete synchronization. Fig. 15 confirms this synchronization when we take the time traces of the 150th oscillator of each layer.

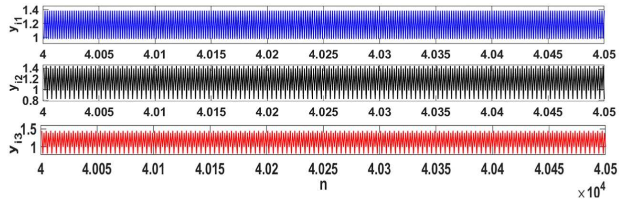

Fig. 13: Time-histories of the 150th oscillator of the first, second and third layers when these layers are out of sync. i=150, σ_{ml}= 0,05, σ_{m}= 0,26, β=0.2 ,α=2.75, P_m=90 , $n_{max=40500}$, the initial conditions are chosen randomly between 0 and 1.

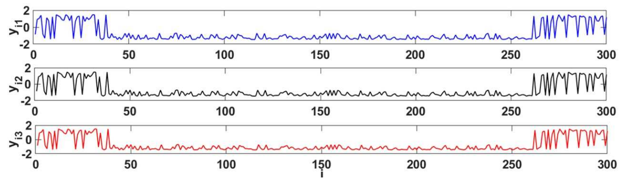

Fig. 14: Complete synchronization of 3 layers with n=40500, σ_{ml}= 0,25, σ_{m}= 0,26, β=0.2 ,α=2.75,P_m=90 ,i=0 to N (with N=300) the initial conditions are chosen randomly between 0 and 1.

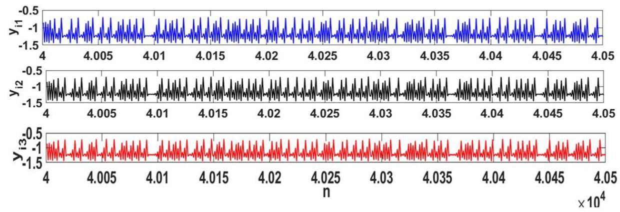

Fig. 15: Time-histories of the 150th oscillator of the first, second and third layers when these layers are synchronized with i=150, σ_{ml}= 0,25, σ_{m}= 0,26, β=0.2 ,α=2.75,P_m=90 ,n_{max}=40500 and the initial conditions are chosen randomly between 0 and 1.

4.2 Study of the synchronization of coupled extended Duffing oscillators in a three-layer network

We used equation 14 to measure the synchronization error between layer 1 and layer 2 (E12) and between layer 1 and layer 3 (E13) of extended coupled Duffing oscillators in a three-layer network (equation 13). Fig. 16 below shows that when σ_{ml} is between 0.02 and 0.14, the errors between the layers are not equal to zero, so the 3 layers are not synchronized. However, there is a zone where layers 1 and 2 are synchronized with each other but not with layer 3 (the red curve E12=0 and E13 different from 0 for σ_{ml} = 0.13). On the other hand, when σ_{ml} is between 0.145 and 0.355, the 3 layers are perfectly synchronized (E12=E13=0). These different scenarios can be confirmed

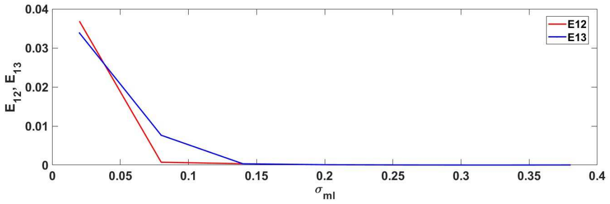

Fig. 16: Synchronization error between layer 1 and 2 : (E12) and layer 1 and 3 : (E13).

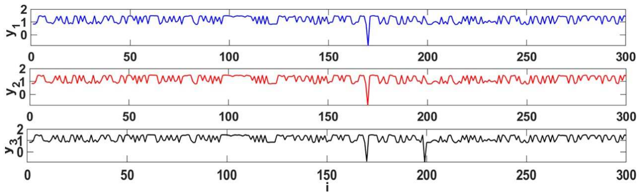

Fig. 17: Partial synchronization of 3 layers with n=40500, σ_{ml}= 0,13, σ_{m}= 0,26, β=0.2 ,α=2.75,P_m=90 , d=0.02,i=0 to N (with N=300) the initial conditions are chosen randomly between 0 and 1.

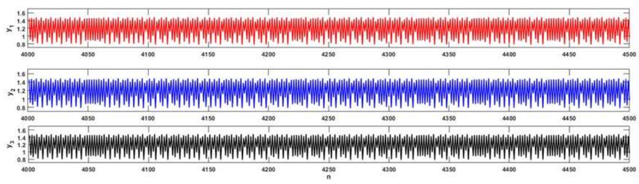

Fig. 18: Time-histories during partial synchronization with σ_{ml}= 0,13, σ_{m}= 0,26, β=0.2 ,α=2.75,P_m=90 , d=0.02,i=0 to N (with N=300) the initial conditions are chosen randomly between 0 and 1.

by plotting the spatial and temporal trace curves in Fig.s 17,18, taking a few values of σ_{ml}.

When σ_{ml} = 0.13, synchronization between the first and second layers is observed (E12=0 curve in blue and red on Fig. 16). All the oscillators in these two layers behave in the same way (see Fig. 17). However, when we take the 200th oscillator of layer 3 (yi3), we notice that it is not synchronized with the other layers. We therefore conclude that there is partial synchronization between the layers.
Time-histories of the 150th oscillators (Fig. 18) of each layer confirm this partial synchronization.

Fig.19 shows that when σ_{ml} =0.25, full synchronization is observed between the first and second layers, as well as between the first and third layers (E12=E13=0). This analysis is confirmed by the fact that all 3-layer oscillators have the same behavior.

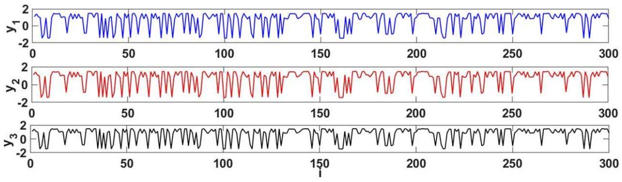

Fig. 19: Complete synchronization n of 3 layers with n=40500, σ_{ml}= 0,25, σ_{m}= 0,26, β=0.2, α=2.75, P_m=90 , d=0.02, i=0 to N (with N=300) the initial conditions are chosen randomly between 0 and 1.

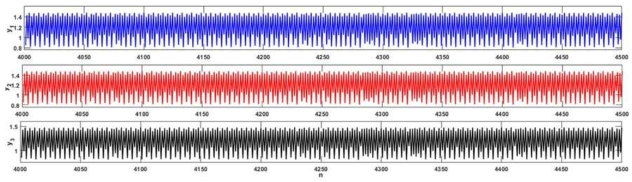

Fig. 20: Time-histories when complete synchronized with σ_{ml}= 0,25, σ_{m}= 0,26, β=0.2, α=2.75, P_m=90 , d=0.02, i=0 to N (with N=300) the initial conditions are chosen randomly between 0 and 1.

Time-histories traces of the 150th oscillator of each layer in Fig. 20 confirm the complete synchronization.

5 Application of Simple Duffing and Extended Duffing network synchronization for information masking

5.1 *Application of simple Duffing network synchronization for information masking*

In this section, we use chaotic state synchronization in multilayer networks to demonstrate that a message sent by the first layer and masked by its chaotic output can be realized. In each layer, we have 300 oscillators where the messages to be transmitted are sent by the various units (oscillators) of the first layer and retrieved by units of the second and third layers. The message transmitted by each first-layer unit is the sum of the chaotic signal and the actual message. Consequently, the way in which messages are dynamically retrieved depends on the synchronization of the layers. In other words, messages cannot be retrieved if there is no synchronization between the layers. The new coupling equations for the three coupled layers are given by equations 15, 16 and 17.

$$\begin{cases} x_i^1(n+1) = f_x^1(x_i,y_i) = y_i^1(n) \\ y_i^1(n+1) = f_y^1(x_i,y_i) + \frac{\sigma_m}{2P_m}\sum_{j=i-P_m}^{i+P_m}\left[f_y^1(x_j,y_j) - f_y^1(x_i,y_i)\right] \\ +\sigma_{ml}\left[f_y^2(x_i,y_i) - 2f_y^1(x_i,y_i) + f_y^3(x_i,y_i)\right] \end{cases} \tag{15}$$

$$\begin{cases} x_i^2(n+1) = f_x^2(x_i, y_i) = y_i^2(n) \\ y_i^2(n+1) = f_y^2(x_i, y_i) + \frac{\sigma_m}{2P_m} \sum_{j=i-P_m}^{i+P_m} \left[f_y^2(x_j, y_j) - f_y^2(x_i, y_i) \right] \\ +\sigma_{ml} \left[f_y^1(z_i, y_i) - 2f_y^2(x_i, y_i) + f_y^3(x_i, y_i) \right] \end{cases} \tag{16}$$

$$\begin{cases} x_i^3(n+1) = f_x^3(x_i, y_i) = y_i^3(n) \\ y_i^3(n+1) = f_y^3(x_i, y_i) + \frac{\sigma_m}{2P_m} \sum_{j=i-P_m}^{i+P_m} \left[f_y^3(x_j, y_j) - f_y^3(x_i, y_i) \right] \\ +\sigma_{ml} \left[f_j^1(z_i, y_i) - 2f_y^3(x_i, y_i) + f_y^2(x_i, y_i) \right] \end{cases} \tag{17}$$

where $z_i(n) = x_i(n) + m(n)$ represents the chaotic signal of the first layer added to the message to be transmitted. The messages recovered at the second and third layers are given by relations 18 and 19 respectively.

$$z_i^2(n) = y_i^1(n) - y_i^2(n) + m(n) \tag{18}$$

$$z_i^3(n) = y_i^1(n) - y_i^3(n) + m(n) \tag{19}$$

Three example signals are used to test the sending and retrieval of messages:

- A square-wave signal sent by the first layer through all the oscillators and recovered by the 150th oscillator;

- A sinusoidal signal sent by the first layer through all oscillators and recovered by the 150th oscillator;

- Two signals m1(n) and m2(n) with different amplitudes sent respectively by the 200 th and 150 th oscillator of the first layer and recovered by the same oscillators of the second and third layers.

To analyze the 3 points mentioned above, we use a value of σ_{ml} leading to desynchronization of 3 layers (Eml different from 0) and a value of σ_{ml} leading to complete synchronization of these layers (Eml $= 0$).

–Square signal

Fig. 21 (a) shows the square-wave signal $m(n)$, while Fig. 21 (b) shows the chaotic signal from the first layer (150th oscillator). Fig. 21 (c) shows the chaotic signal mixed with the real signal to be transmitted $(y_1(150)(n) + m(n))$. Using the value $\sigma_{\text{ml}} = 0.05$, for which the message-free system is not synchronized (Fig. 11), Figs. 21 (d) and (e) show what is recovered at the second and third layers. The message is not recovered. However, when the coupling value is chosen as that for which the layers are synchronized, for example, $\sigma_{\text{ml}} = 0.25$ (as seen in Fig. 11), the message is recovered, as shown in Fig. 22. The signal recovered by the second and third layers corresponds to the original $m(n)$ signal. However, the recovered signal contains noise, which can be reduced by using an appropriate filter [25].

–Sine signal

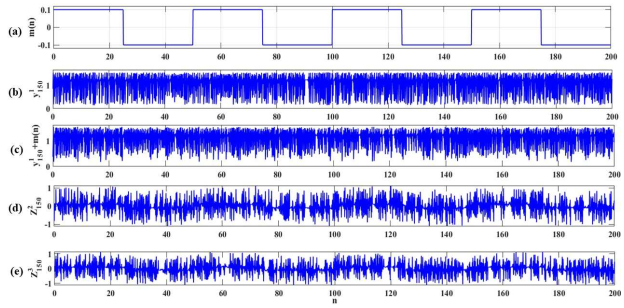

Fig. 21: Different types of Time-histories when there is no synchronization between layers for an inter-layer coupling strength σ_{ml} = 0.05. (a) square-wave signal m(n) to be transmitted by the first layer; (b) chaotic signal from the first layer y1(150) (n); (c) chaotic signal added to the transmitted signal y1(150) (n) +m(n); (d) information signal recovered by the second layer z2 (150) (n) and (e) information signal recovered by the third layer z3 (150) (n).

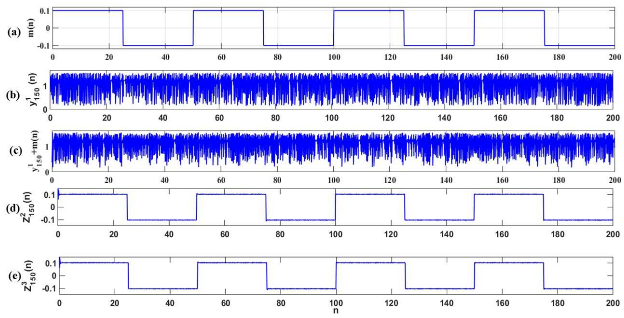

Fig. 22: Different types of Time-histories when there is synchronization between the layers for an inter-layer coupling strength σ_{ml} = 0.25. (a) square-wave signal m(n) to be transmitted by the first layer; (b) chaotic signal from the first layer y1(150)(n); (c) chaotic signal added to the transmitted signal y1(150)(n) +m(n); (d) information signal recovered by the second layer z2 (150)(n) and (e) information signal recovered by the third layer z3 (150)(n).

A second example is a sine message. We observe that, as in the case of the square-wave signal, when there is no synchronization of the three distant layers (σ_{ml}= 0.05), we are unable to recover the original signal. The signal is lost on layer 2 chaos, for example (see Fig. 23). However, when the coupling is appropriately chosen so as to have layer synchronization σ_{ml}= 0.25, the message is recovered at the second and third layers as shown in Fig. 24.

–Two messages sent simultaneously with different amplitudes

In this section, we sent two messages simultaneously on the 200th and 150th oscillators of the first layer. We

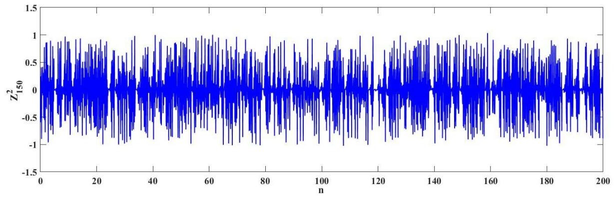

Fig. 23: Time-histories when there is no interlayer synchronization for an interlayer coupling strength σ_{ml}= 0.05. Message retrieved by the 150th oscillator Z2 (150).

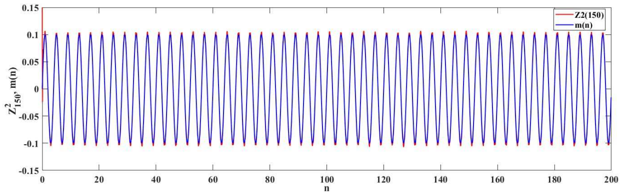

Fig. 24: Time-histories trace when layers are synchronized for an inter-layer coupling force σ_{ml}= 0.25. Message retrieved by the 150th oscillator Z2 (150) in red and message sent m(n) in blue.

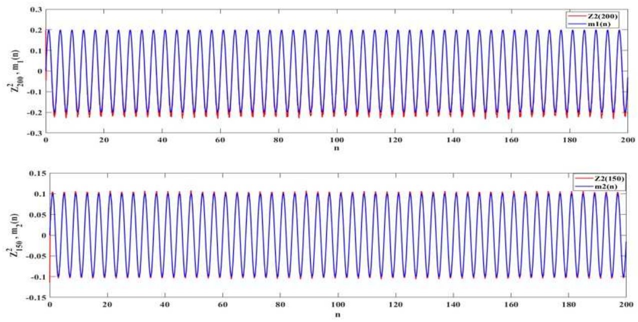

Fig. 25: Messages retrieved respectively by the 200th and 150th oscillator when there is interlayer synchronization for an interlayer coupling strength with σ_{ml}= 0.25.

can see that perfect recovery is achieved by the second and third layers at a value of $\sigma_{\mathrm{ml}} = 0.25$ (Fig. 25). This is because the 3 layers are perfectly synchronized. However, when the layers are not synchronized, messages get mixed up in the chaotic 2nd and 3rd layer when $\sigma_{\mathrm{ml}} = 0.05$ (Fig. 26).

5.2 Application of extended Duffing network synchronization for information masking

Using the same principle as in the case of a simple Duffing network, Fig. 27 (a) shows the square-wave

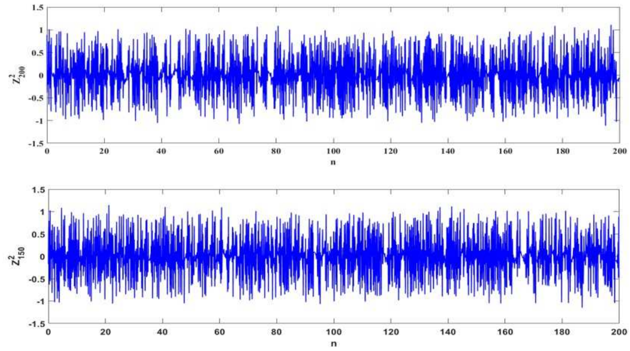

Fig. 26: Messages recovered by the 200th and 150th oscillators respectively when there is no interlayer synchronization for an interlayer coupling strength σ_{ml}= 0.05

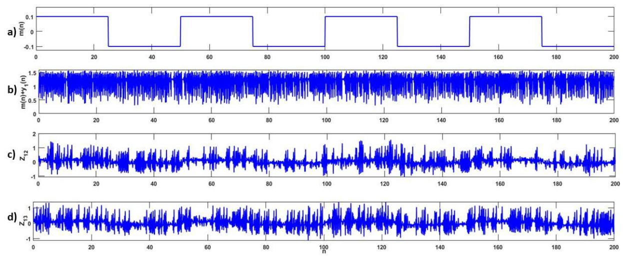

Fig. 27: Different types of time-histories when there is no synchronization between layers for an inter-layer coupling strength σ_{ml}= 0.06. (a) square-wave signal m(n) to be transmitted by the first layer; (b) chaotic signal added to the transmitted signal y1(150)(n) +m(n); (c) information signal recovered by the second layer z2 (150)(n) and (d) information signal recovered by the third layer z3 (150)(n)..

signal $m(n)$, while Fig. 27 (b) shows the chaotic signal from the first layer (150th oscillator). Fig. 27 (c) shows the chaotic signal mixed with the actual signal to be transmitted ($\mathrm{y1(150)(n) + m(n)}$). Using the value $\sigma_{\mathrm{ml}} = 0.06$ for which there is no synchronization (Fig. 16), Fig.s 27 (d) and (e) show what is recovered at the second and third layers. The message is not recovered. It is lost in the chaos of the system. On the other hand, when the coupling value is chosen as that for which the layers are partially synchronized, e.g. $\sigma_{\mathrm{ml}} = 0.13$ (as shown in Fig. 16), the message is not fully recovered, as shown in Fig. 28. We can still distinguish the message from the chaos. On the other hand, when the coupling value is chosen to obtain full synchronization, for example $\sigma_{\mathrm{ml}} = 0.25$ (as shown in Fig. 16), the signal recovered by the second and third layers corresponds well to the original $m(n)$ signal (see Fig. 29). However, the recovered signal contains noise that can be reduced using a filter.

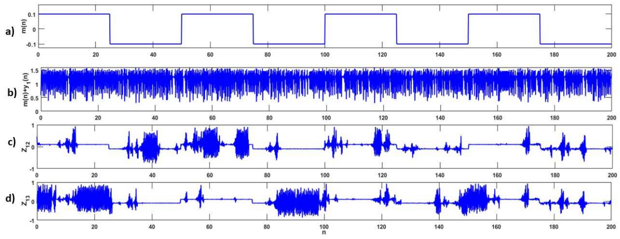

Fig. 28: Different types of time-histories when there is partial synchronization between layers for an inter-layer coupling strength $\sigma_{ml} = 0.13$. (a) square-wave signal m(n) to be transmitted by the first layer; (b) chaotic signal added to the transmitted signal y1(150) (n) +m(n); (c) information signal recovered by the second layer z2 (150) (n) and (d) information signal recovered by the third layer z3 (150) (n).

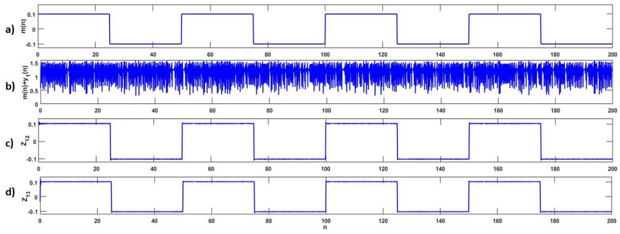

Fig. 29: Different types of time-histories when there is complete synchronization between layers for an inter-layer coupling strength $\sigma_{ml} = 0.25$. (a) square-wave signal m(n) to be transmitted by the first layer; (b) chaotic signal added to the transmitted signal y1(150) (n) +m(n); (c) information signal recovered by the second layer z2 (150) (n) and (d) information signal recovered by the third layer z3 (150)(n).

6 Conclusion

The synchronization of coupled simple and extended discrete Duffing oscillators in a 3-layer network was numerically investigated in this paper. Initially, the characterization of the one-dimensional simple Duffing and one-dimensional extended Duffing discrete oscillator has enabled us to find the values where the control parameters give rise to chaos. It was then demonstrated that synchronization phenomena can be observed in a 3-layer network of simple and extended Duffing discrete oscillators for selected values of the coupling strength. For the application to chaos cryptography, it was demonstrated that when the three layers are not synchronized, the transmitted message gets lost in the chaotic signal of the first layer and can no longer be decrypted by the second and third layers. On the other hand, when the three distant layers are synchronized, the message can be recovered by the second and third layers. A study of the influence of fractional derivation on the discrete oscillator of simple Duffing and extended Duffing was presented. The study showed that a small fractional order reduced the area in the chaotic zone.

References

[1] P. K. Roy, C. Hens, I. Grosu, S. K. Dana. Engineering generalized synchronization in chaotic oscillators. Chaos 21, 013106 (2011).

[2] B. Nana, P. Woafo. Synchronization in a ring of four mutually coupled Van der Pol oscillators: theory and experiment. Phys Rev E 74, 1–8 (2006).

[3] K. Bidesh, Bera, G. Dibakar, L. Muthusamy L. Chimera states in bursting neurons. Phys Rev E 91, 012205 (2015).

[4] I. A. Shepelev, T. E. Vadivasova. Synchronization in multipslex networks of chaotic oscillators with frequency mismatch. Chaos, Solitons and Fractals 147, 110882 (2021).

[5] K. Y. Chembo, P. Woafo. Transitions from spatiotemporal chaos to cluster and complete synchronization states in a shift-invariant set of coupled nonlinear oscillators. Phys Rev E 67, 046205 (2003).

[6] B. K. Bera S. Majhi, D. Ghosh, M. Perc. Chimera states: Effects of different coupling topologies, Europhysics Letters, 118, 10001 (2017).

[7] Y. Kuramoto, D. Battogtokh. Coexistence of coherence and incoherence in nonlocally coupled phase oscillators, Nonlinear Phenomena in Complex Systems, 5, 380–385 (2002).

[8] A. S., Zakharova, S. Jalan. Non-identical multiplexing promotes chimera states, Chaos, Solitons and Fractals 106, 56–60 (2018).

[9] A. S. Carlos, Batista, L. Ricardo, Viana. Quantifying coherence of chimera states in coupled chaotic systems, Physica A, 526, 120869 (2019).

[10] M. De Domenico, A. Solé-Ribalta, E. Cozzo, M. Kivelä, Y. Moreno, M. A. Porter, S. Gómez, A. Arenas. Mathematical formulation of multilayer networks, Phys. Rev. X, 041022 (2013)

[11] M. Kivelä, A. Arenas, M. Barthelemy, J. P. Gleeson, Y. Moreno, M. A. Porter, Multilayer networks, J. Complex Netw. 2, 203–271 (2014)

[12] S. Boccaletti, G. Bianconi, R. Criado, C. I. Del Genio, J. Gómez-Gardenes, M. Romance, I. Sendina-Nadal, Z. Wang, M. Zanin, The structure and dynamics of multilayer networks, Phys. Rep. 544, 1–122 (2014)

[13] L. V. Gambuzza, M. Frasca , J. Gómez-GardeñesJ. Intra-layer synchronization in multiplex networks, Europhys. Lett. 110, 20010 (2015).

[14] R. Sevilla-Escoboza, I. Sendiña-Nadal, I. Leyva, R. Gutiérrez, J. M. Buldú, S. Boccaletti, Inter-layer synchronization in multiplex networks of identical layers, Chaos 26, 065304 (2016).

[15] Md. S. Anwar, S. Rakshit, D. Ghosh, E. M. Bollt. Stability analysis of intralayer synchronization in time-varying multilayer networks with generic coupling functions, Phys. Rev. E 105, 024303 (2022).

[16] S. Ghosh, A. Kumar, A. Zakharova, S. Jalan, Birth and death of chimera:interplay of delay and multiplexing, Europhys. Lett. 115, 60005 (2016)

[17] M. Winkler, J. Sawicki, I. Omelchenko, A. Zakharova, V. Anishchenko, E. Schöll. Relay synchronization in multiplex networks of discrete maps. EPL, 126, 50004 (2019).
[18] M. De Domenico, A. Solé-Ribalta, E. Cozzo , M. Kivelä, Y. Moreno, M.A. Porter. A. Mathematical formulation of multilayer networks. Phys Rev. X. 3, 041022 (2013).
[19] E. Rybalova, G. Strelkova, E. Scholl, V. Anishchenko. Relay and complete synchronization in heterogeneous multiplex networks of chaotic maps. Chaos, 30, 061104 (2020).
[20] I. Leyva, R. Sevilla-Escoboza, I. Sendiña-Nadal, R. Gutiérrez, J. Buldú, S. Boccaletti. Inter-layer synchronization in non-identical multi-layer networks. Sci. Rep. 7, 45475 (2017).
[21] L. J. Kovarev, K. S. Halle, K. Eckert, U. Parlitz ,L. O. Chua. Experimental demonstration of secure communications via chaotic synchronization. International Journal of Bifurcation and Chaos 2, 709-713, 1992.
[22] G. Perez, H. A. Cerdeira. Extracting messages masked by chaos. Physical Review Letter 74, 1970-1973 (1995).
[23] P. Woafo. Transitions to Chaos and synchronization in a nonlinear emitter-receiver system. Physics Letters A 267, 31-39 (2000).
[24] Zhou, Lili, F. Tan, F. Yu. A Robust Synchronization-Based Chaotic Secure Communication Scheme with Double-Layered and Multiple Hybrid Networks, IEEE Systems Journal 14, 2508-2519 (2020).
[25] A. Ghasemzadeh, E. Esmaeili. A novel method in audio message encryption based on a mixture of chaos function. Int J Speech Technol, 20, 829–837 (2017).
[26] B. Nana, Woafo P, Domngang P. Chaotic synchronization with experimental application to secure communications. Communications in Nonlinear Science and Numerical Simulation, 14, 2266-2276 (2009).
[27] Her-Terng Yau, Yu-Chi Pu, Simon Cimin Li. Application of a Chaotic Synchronization System to Secure Communication. Information Technology and Control, 41:3 (2012).
[28] Sifeu Takougang Kingni, Jimmi Hervé Talla Mbé, Paul Woafo. Semiconductor lasers driven by self-sustained chaotic electronic oscillators and applications to optical chaos cryptography. Chaos, 22, 033108 (2012).
[29] L. Zhou, F. Tan, F. Yu. A Robust Synchronization-Based Chaotic Secure Communication Scheme with Double-Layered and Multiple Hybrid Networks. IEEE Systems Journal 14, 2508-2519 (2020).
[30] Lili Zhou, Xiaohui Li, Fei Tan, Huang Yi, Weina Ma. A two-layer networks-based audio encryption/decryption scheme via fixed-time cluster synchronization. Soft Comput, 26, 9761–9774 (2022).
[31] Liu H, Wan H, Tse CK, Lu Jan. encryption scheme based on synchronization of two-layered complex dynamical networks. IEEE Trans Circuits Syst I 63, 2010-2021 (2016).
[32] Kanan M. Babanli, Rana Ortac Kabaoglu, Synchronization of fuzzy-chaotic systems with Z-controller in secure communication, Information Sciences 657, 0020-0255 (2024).
[33] H. Natiq, A. Roy, S. Banerjee, A. P. Misra, A. Fataf. Enhancing chaos in multistability regions of Duffing map for an asymmetric image encryption algorithm. Soft Computing 27, 19025–19043 (2023).
[34] O. Megherbi, H. Hamiche, S. Djennoune, M. Bettayeb M. A new contribution for the impulsive synchronization of fractional-order discrete-time chaotic systems. Nonlinear Dyn. 90, 1519–1533 (2017).
[35] Z. Kalsoubé, M. H. Ahamat, Y. K. Mahamoud, P. Woafo, Chaos in new polynomial discrete logistic maps with fractional derivative and applications for text encryption. Appl. Math. Inf. Sci.17, 807-816 (2023).
[36] Z. Yong, Basic theory of fractional differential equations, World scientific (2023).
[37] A. A. Khennaoui, A. Ouannas, S. Momani, O. A. Almatroud, M.M. Al-Sawalha, M.M. Boulaaras, V. T. Pham, Special Fractional-Order Map and Its Realization, Mathematics 10, 4474 (2022).
[38] L. Diabi, A. Ouannas, A. Hioual, G. Grassi and S. Momani, The Discrete Ueda System and Its Fractional Order Version: Chaos, Stabilization and Synchronization, Mathematics 13, 239 (2025).

Ahamat Mahamat Hassane received the M.S degree in Telecommunication from National Institute of Science and Technology of Abéché, Chad, in 2019, where his currently pursuing the Ph.D. He is currently investigating the synchronization of multi-layer nonlinear discrete oscillator networks and their application to data security.

Kalsouabe Zoukalné received his PhD in Telecommunications from the University of N'Djamena, Chad, in January 2025. He is assistant at the Virtual University of Chad since 2020 and an external member of Laboratory of Modelling and Simulation in Engineering, Biomimetics and Prototypes (LAMSEBP).His research interests include discrete chaotic systems and their application to cryptography, mobile networks, and artificial intelligence applied to cybersecurity.

Yaya Dagal Dari, CAMES Senior Lecturer, Research teacher at National Institute of Science and Technology of Abéché INSTA/TCHAD. He is also the Head of the Research Department and coordinator of the PEA-TCHAD project. He was Head of the Department of Electrical Engineering from 2013 to 2017. Currently, he is the Director General of INSTA. Yaya DAGAL received his PhD in Photonic Optics and Microwave from Jean Monnet University of Saint Etienne (France) in 2014. His research fields are Electronics, Optronics, Systems and Microwave.

Paul Woafo received the Ph.D. degree in physics from the University of Yaoundé I, in 1992, and the Doctorat d'Etat degree in physics in 1997. He is Full Professor at the University of Yaoundé I since 2005, and heads the Laboratory of Modelling and Simulation in Engineering, Biomimetics and Prototypes (LAMSEBP). He is also an external member of the Applied Physics Group, Vrije Universiteit Brussel, Belgium. He is authors of 280 refereed articles in international journals. He was awarded the TWAS Prize for Young Scientists in 2004. His research interests involve the nonlinear dynamics in optoelectronics, electromechanics, electronic, biological and chaos cryptography systems. He was a member of the International Union of Pure and Applied Physics (IUPAP) Commission for statistical physics (C3). He was awarded the 2020 medal of the IUPAP Commission of Physics for development. He is a Founding Member and the former President of the Cameroon Physical Society (CPS), member of the board of the African Physical Society (AfPS), and the Dean of the College of Mathematics and Physical Sciences, Cameroon Academy of Sciences. He was an Associate member (junior, regular and senior) of the Abdus Salam International Center for Theoretical Physics (1995-2013). He is Georg Forster Fellow of the Humboldt Foundation, Germany.